Dispersion and line shape of plasmon satellites in one, two, and three dimensions

Derek Vigil-Fowler,[1] Steven G. Louie,[2,*] and Johannes Lischner[3,*]
[1]*National Renewable Energy Laboratory, Golden, Colorado 80401, USA*
[2]*Department of Physics, University of California, Berkeley, California 94720, USA*
and Materials Sciences Division, Lawrence Berkeley National Laboratory, Berkeley, California, USA
[3]*Department of Physics and Department of Materials, and the Thomas Young Centre for Theory and Simulation of Materials, Imperial College London, London SW7 2AZ, United Kingdom*
(Received 18 December 2015; revised manuscript received 8 June 2016; published 27 June 2016)

Using state-of-the-art many-body Green's function calculations based on the *GW* plus cumulant approach, we analyze the properties of plasmon satellites in the electron spectral function resulting from electron-plasmon interactions in one-, two-, and three-dimensional systems. Specifically, we show how their dispersion relation, line shape, and linewidth are related to the properties of the constituent electrons and plasmons. To gain insight into the many-body processes giving rise to the formation of plasmon satellites, we connect the *GW* plus cumulant approach to a many-body wave-function picture of electron-plasmon interactions and introduce the coupling-strength-weighted electron-plasmon joint density states as a powerful concept for understanding plasmon satellites.

DOI: 10.1103/PhysRevB.93.235446

Introduction. The interaction of electrons with bosons is of fundamental importance for many phenomena in condensed matter physics, plasma physics, and cold atom physics. Recently, there has been great interest in the coupling of electrons and plasmons, which are collective excitations describing quantized oscillations of the charge density. For example, the decay of plasmons into energetic or "hot" electron-hole pairs in metallic surfaces and nanoparticles, which is triggered by electron-plasmon coupling, has led to a new generation of plasmonic devices for photovoltaics and photocatalysis [1–3].

Satellite features in the spectral function of electrons are another consequence of electron-plasmon interactions. Such plasmon satellites have long been known in core-electron photoemission spectra [4,5]. In recent years, valence band plasmon satellites, which were observed experimentally in three-dimensional metals and semiconductors [6–9], but also in two-dimensional systems, such as doped graphene and semiconductor quantum-well electron gases [10–12], received much attention.

To analyze and design the properties of plasmon satellites for photonics and plasmonics applications, an accurate, material-specific theoretical description of electron-plasmon interactions is needed. This is achieved by the *GW* plus cumulant (*GW*+C) approach [13,14], where the cumulant expansion of the electron Green's function G is truncated at second order in the screened Coulomb interaction W. *GW*+C calculations yielded good agreement with experimental photoemission and tunneling spectra in a wide range of physical systems [6–8,15–17] and also with highly accurate coupled-cluster Green's function calculations [18].

While Green's function methods, such as the *GW*+C approach, often produce highly accurate results, gaining intuition and insights into the underlying many-body processes can be difficult. In this paper, we develop a complementary many-body wave-function-based approach for plasmonic (and more generally, bosonic) satellites in the electron spectral function which offers a clear and simple physical picture of electron-plasmon interactions and leads to insights into the results of *GW*+C calculations. Specifically, this approach reveals that the concepts of satellite dispersion, satellite line shape, and satellite linewidth are closely related, explains why in three-dimensional materials the plasmon satellite band structure looks like a shifted copy of the quasiparticle band structure, and demonstrates that previous models of plasmon satellites in three dimensions are oversimplified and cannot be applied to lower-dimensional systems. We present results for three-dimensional [silicon and the three-dimensional electron gas (3DEG)], two-dimensional (doped graphene), and one-dimensional [the one-dimensional electron gas (1DEG)] systems.

Green's function theory. The electron spectral function is related to many observables, such as the tunneling and photoemission spectrum, and the contribution $A^{\mathrm{IP}}_{\boldsymbol{k}}(\omega)$ (with $\boldsymbol{k}$ denoting the wave vector and we omit a band index) describing the removal of an electron is given by [19,20]

$$A^{\mathrm{IP}}_{\boldsymbol{k}}(\omega) = \sum_{\lambda} |\langle N-1,\lambda|c_{\boldsymbol{k}}|\mathrm{GS}\rangle|^2 \delta(\omega + E_{N-1,\lambda} - E_{\mathrm{GS}}), \quad (1)$$

where $|\mathrm{GS}\rangle$ and E_{GS} denote the ground-state wave function and energy of the N-electron system, respectively, and $|N-1,\lambda\rangle$ and $E_{N-1,\lambda}$ denote the eigenstates and energies of the $(N-1)$-electron system.

The spectral function is related to the one-electron Green's function $G_{\boldsymbol{k}}(\omega)$ via $A_{\boldsymbol{k}}(\omega) = 1/\pi \times |\mathrm{Im}G_{\boldsymbol{k}}(\omega)|$. Within the generalized *GW*+C approach, the retarded Green's function is expressed as a function of time t via [21]

$$G_{\boldsymbol{k}}(t) = -i\Theta(t) e^{-iE^{\mathrm{HF}}_{\boldsymbol{k}} t + C_{\boldsymbol{k}}(t)}, \quad (2)$$

where $E^{\mathrm{HF}}_{\boldsymbol{k}}$ denotes the Hartree-Fock orbital energy (given by $E^{\mathrm{HF}}_{\boldsymbol{k}} = \epsilon_{\boldsymbol{k}} + \Sigma^{\mathrm{X}}_{\boldsymbol{k}} - V^{xc}_{\boldsymbol{k}}$ with $\epsilon_{\boldsymbol{k}}$, $V^{xc}_{\boldsymbol{k}}$, and $\Sigma^{\mathrm{X}}_{\boldsymbol{k}}$ denoting the mean-field orbital energy, the mean-field exchange-correlation potential, and the bare exchange self-energy, respectively).

*jlischner597@gmail.com

Also, $C_{\boldsymbol{k}}(t)$ is the cumulant function given by

$$C_{\boldsymbol{k}}(t) = \frac{1}{\pi}\int d\omega |\mathrm{Im}\Sigma_{\boldsymbol{k}}(\omega + E_{\boldsymbol{k}})| \frac{e^{-i\omega t} + i\omega t - 1}{\omega^2}, \quad (3)$$

where $\Sigma_{\boldsymbol{k}}(\omega)$ denotes the GW self-energy [22,23] and $E_{\boldsymbol{k}}$ is the GW quasiparticle energy.

To gain physical understanding, it is useful to separate the cumulant function into a satellite contribution $C^{\mathrm{sat}}_{\boldsymbol{k}}(t)$, which contains the $e^{-i\omega t}$ term in Eq. (3), and a quasiparticle contribution, which contains the $(i\omega t - 1)$ term. Expanding the Green's function in powers of $C^{\mathrm{sat}}_{\boldsymbol{k}}$ leads to a representation of the spectral function as the sum of a quasiparticle contribution $A^{\mathrm{qp}}_{\boldsymbol{k}}$ and an infinite series of plasmon satellite contributions $A^{(m)}_{\boldsymbol{k}}$ (with m denoting the number of plasmons that are created in the shake-up process). Specifically, the first satellite contribution can be expressed as

$$A^{(1)}_{\boldsymbol{k}}(\omega) = \int d\omega' C^{\mathrm{sat}}_{\boldsymbol{k}}(\omega - \omega') A^{\mathrm{qp}}_{\boldsymbol{k}}(\omega'). \quad (4)$$

Approximating $A^{\mathrm{qp}}_{\boldsymbol{k}}(\omega) \approx Z_{\boldsymbol{k}}\delta^{(\Gamma_{\boldsymbol{k}})}(\omega - E_{\boldsymbol{k}})$ with $Z_{\boldsymbol{k}}$ denoting the renormalization factor and $\delta^{(\Gamma)}$ being a Lorentzian of width Γ, we find that $A^{(1)}_{\boldsymbol{k}}(\omega) \approx Z_{\boldsymbol{k}}/\pi \times \mathrm{Im}\Sigma_{\boldsymbol{k}}(\omega)/(\omega - E_{\boldsymbol{k}})^2$.

Evaluating Eq. (4) requires the calculation of the imaginary part of the GW self-energy. To clarify the physical picture, we use the self-energy of a homogeneous electron system in D dimensions with a plasmon-pole model for the dielectric response. With these assumptions, the electron-removal part of the self-energy is given by [23]

$$\mathrm{Im}\Sigma^{\mathrm{IP}}_{\boldsymbol{k}}(\omega) = \frac{\pi}{L^D}\sum_{\boldsymbol{q}} \lambda_{\boldsymbol{q}} v_{\boldsymbol{q}} \delta(\omega - E_{\boldsymbol{k}-\boldsymbol{q}} + \omega_{\boldsymbol{q}}), \quad (5)$$

where $v_{\boldsymbol{q}}$ denotes the Coulomb interaction in D dimensions and $\omega_{\boldsymbol{q}}$ and $\lambda_{\boldsymbol{q}}$ are the plasmon dispersion relation and the plasmon strength, respectively. Also, L is the linear extension of the system and $\boldsymbol{k} - \boldsymbol{q}$ corresponds to a hole state.

Inserting Eq. (5) into the expression for $A^{(1)}_{\boldsymbol{k}}$ yields

$$A^{(1)}_{\boldsymbol{k}}(\omega) = \frac{Z_{\boldsymbol{k}}}{L^D}\sum_{\boldsymbol{q}} \frac{g^2_{\boldsymbol{q}}}{(E_{\boldsymbol{k}} - E_{\boldsymbol{k}-\boldsymbol{q}} - \omega_{\boldsymbol{q}})^2}\delta(\omega - E_{\boldsymbol{k}-\boldsymbol{q}} + \omega_{\boldsymbol{q}}), \quad (6)$$

where we introduced the electron-plasmon coupling strength $g^2_{\boldsymbol{q}} = \lambda_{\boldsymbol{q}} v_{\boldsymbol{q}}$. Equation (6) shows that the satellite contribution to the spectral function closely related to the coupling-strength-weighted electron-plasmon joint-density of states $J_{\boldsymbol{k}}(\omega) = 1/L^D \times \sum_{\boldsymbol{q}} g^2_{\boldsymbol{q}}\delta(\omega - E_{\boldsymbol{k}-\boldsymbol{q}} + \omega_{\boldsymbol{q}})$ comprising only plasmon-hole pairs with total momentum $\boldsymbol{k}$.

Wave-function theory. We will now demonstrate that the expression for the satellite contribution to the spectral function from GW+C [Eq. (6)] can also be derived by considering the effective electron-plasmon Hamiltonian

$$H_{el-pl} = \sum_{\boldsymbol{k}} E_{\boldsymbol{k}} c^\dagger_{\boldsymbol{k}} c_{\boldsymbol{k}} + \sum_{\boldsymbol{q}} \omega_{\boldsymbol{q}} a^\dagger_{\boldsymbol{q}} a_{\boldsymbol{q}} \quad (7)$$

$$+ \sum_{\boldsymbol{q},\boldsymbol{k}} \frac{g_{\boldsymbol{q}}}{\sqrt{L^D}} c^\dagger_{\boldsymbol{k}-\boldsymbol{q}} c_{\boldsymbol{k}} (a_{\boldsymbol{q}} + a^\dagger_{-\boldsymbol{q}}), \quad (8)$$

where $c_{\boldsymbol{k}}$ and $a_{\boldsymbol{q}}$ are destruction operators for quasiparticles and plasmons, respectively. In this Hamiltonian, the first term describes a set of noninteracting quasiparticles, the second term describes a set of noninteracting plasmons (or more generally, bosons), and the third term captures the interaction between quasiparticles and plasmons.

This electron-boson Hamiltonian plays a fundamental role in the theory of electron-phonon interactions, but computing accurate spectral functions is difficult [19,24,25]. At intermediate coupling strengths, different types of perturbation theory give significantly different results: When compared to highly accurate path-integral calculations, the self-consistent Brillouin-Wigner perturbation theory yields substantially *worse* results than standard Rayleigh-Schrödinger perturbation theory [19].

For electron-plasmon interactions, Lundqvist demonstrated [24] that the application of Brillouin-Wigner perturbation theory to H_{el-pl} results in the Dyson equation of the GW approach. Solving this equation, he found *two* solutions. While the first solution corresponds to a standard quasiparticle excitation, he assigned the second solution to a novel particle, the *plasmaron*, a strongly coupled, coherent hole-plasmon state. Despite several reports claiming the observation of the plasmaron [10,11], it has become clear recently that no such excitation exists in known materials and that its spurious prediction signals the inability of the GW method (and, equivalently, the Brillouin-Wigner perturbation theory) to describe plasmon satellites [6,7,15,16].

Motivated by its accurate description of electron-phonon interactions, we now apply Rayleigh-Schrödinger perturbation theory to H_{el-pl}. Without electron-plasmon interactions, i.e., for $g_{\boldsymbol{q}} = 0$, the eigenstates of the $(N-1)$-electron system are simply $c_{\boldsymbol{k}}|\mathrm{GS}\rangle$ (with energy $E_{\mathrm{GS}} - E_{\boldsymbol{k}}$) and $a^\dagger_{\boldsymbol{q}} c_{\boldsymbol{k}-\boldsymbol{q}}|\mathrm{GS}\rangle$ (with energy $E_{\mathrm{GS}} - E_{\boldsymbol{k}-\boldsymbol{q}} + \omega_{\boldsymbol{q}}$) [26]. Only the state $c_{\boldsymbol{k}}|\mathrm{GS}\rangle$ gives a contribution to Eq. (1) and the resulting spectral function has a single delta-function peak and no satellite features.

Next, we include electron-plasmon interactions using first-order Rayleigh-Schrödinger perturbation theory. The noninteracting states that lie in the energy region of the first satellite are the hole-plasmon pairs $a^\dagger_{\boldsymbol{q}} c_{\boldsymbol{k}-\boldsymbol{q}}|\mathrm{GS}\rangle$. Including the hole-plasmon coupling yields

$$a^\dagger_{\boldsymbol{q}} c_{\boldsymbol{k}-\boldsymbol{q}}|\mathrm{GS}\rangle \rightarrow \left[a^\dagger_{\boldsymbol{q}} c_{\boldsymbol{k}-\boldsymbol{q}} + \frac{1}{\sqrt{L^D}}\frac{g_{\boldsymbol{q}}}{E_{\boldsymbol{k}} - E_{\boldsymbol{k}-\boldsymbol{q}} + \omega_{\boldsymbol{q}}} c_{\boldsymbol{k}} + \cdots\right] \times |\mathrm{GS}\rangle; \quad (9)$$

i.e., the hole-plasmon pair state acquires a quasiparticle component, which makes this state "visible" in the spectral function as a satellite structure. Inserting Eq. (9) into Eq. (1), we recover Eq. (6) for the plasmon satellite contribution to the electron spectral function. This analysis shows clearly that no single, coherent hole-plasmon state is formed, but instead the satellite is comprised of a large number of incoherent, weakly interacting hole-plasmon pairs.

Plasmon satellites in three dimensions. We first study the properties of plasmon satellites in the 3DEG. In this system, the plasmon dispersion is parabolic at small wave vectors, i.e., $\omega_{\boldsymbol{q}} = \omega_0 + \beta q^2$ [20], and we assume that also the quasiparticle dispersion is parabolic, i.e., $E_{\boldsymbol{k}} = \alpha k^2$.

With these assumptions, we can *analytically* compute the coupling-constant-weighted electron-plasmon joint density of states, which is closely related to the satellite contribution

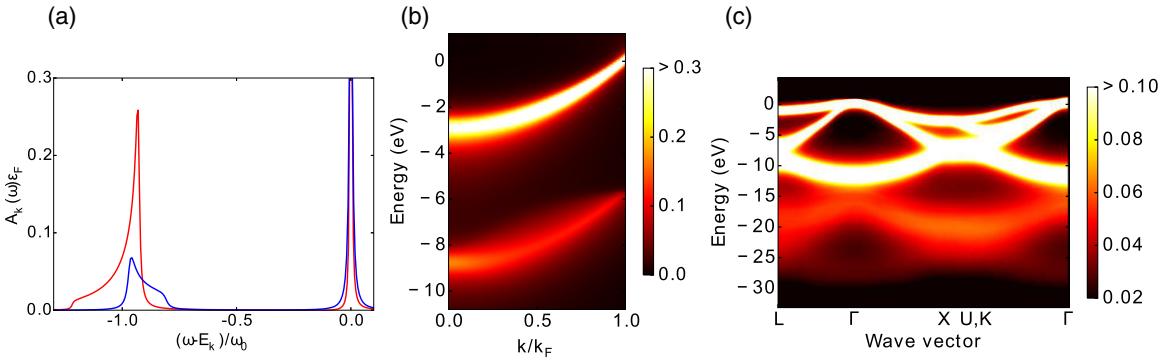

FIG. 1. (a) *GW* plus cumulant spectral functions of the three-dimensional electron gas at $\boldsymbol{k} = 0$ for $r_s = 1.0$ (red curve) and $r_s = 3.0$ (blue curve). (b) Spectral functions (in 1/eV) of the three-dimensional electron gas at $r_s = 4.0$ (corresponding to metallic sodium) from *GW* plus cumulant theory. (c) Spectral functions (in 1/eV) of silicon from *ab initio GW* plus cumulant theory calculations.

$A^{(1)}_{\boldsymbol{k}}(\omega)$ to the spectral function (see Appendix). For $\boldsymbol{k} = 0$, we find

$$J_{\boldsymbol{k}=0}(\omega) = \frac{\omega_0}{2\pi} \frac{\Theta(\mathrm{sgn}(\alpha-\beta)[\omega+\omega_0])}{\sqrt{|(\alpha-\beta)(\omega+\omega_0)|}}. \qquad (10)$$

This result shows that the satellite feature is peaked at $\omega = -\omega_0$; i.e., the satellite is shifted from the quasiparticle energy by the lowest plasmon energy ω_0. Moreover, the satellite exhibits a highly *asymmetric* line shape, which depends sensitively on the *relative magnitudes of the plasmon and quasiparticle effective masses* [given by $m^*_{pl} = 1/(2\beta)$ and $m^*_{qp} = 1/(2\alpha)$, respectively]: if β is larger α, the satellite peak has a tail towards higher binding energies (i.e., away from the Fermi energy). If α is greater than β, the tail is towards lower binding energies. If the effective masses are equal, the satellite structure is symmetric.

Equation (10) predicts the occurrence of a drastic change in the satellite line shape as function of the Wigner-Seitz radius r_s. While the quasiparticle effective mass only has a weak dependence on r_s and may be approximated by its noninteracting value, i.e., $\alpha = 0.5$ (in atomic units) [23], the plasmon effective mass depends sensitively on r_s. Within the random-phase approximation (RPA), we find $\beta \approx 0.64/\sqrt{r_s}$ [20]. At small r_s, β is large and the tail of the satellite extends to higher binding energies. For $r_s \gtrsim 1.6$, β is smaller than α and the tail of the satellite extends to lower binding energies. Figure 1(a) shows the *GW*+C spectral functions for the 3DEG with $r_s = 1.0$ and $r_s = 3.0$ obtained with a plasmon-pole model. It can clearly be seen that the tails of the satellites extend into different directions.

In combination with angle-resolved photoemission spectroscopy (ARPES), the above analysis imposes useful limits on the value of the plasmon effective mass. While ARPES experiments do not measure the plasmon dispersion, they can determine both the quasiparticle effective mass and the satellite line shape. Depending on the direction of the satellite tail [see Fig. 1(a)], the plasmon effective mass must be either smaller or larger than the quasiparticle effective mass. This approach is particularly useful in multiband systems, where each band leads to an additional constraint on the plasmon effective mass.

The satellite line shape from *full GW*+C calculations is more symmetric than predicted by Eq. (10) since additional broadening mechanisms arising from finite quasiparticle linewidths [see Eq. (4)] and finite plasmon linewidths (for example, caused by Landau damping [27]) are taken into account. The total linewidth of the satellite may thus be approximated as the sum of the widths of the coupling-strength-weighted hole-plasmon joint density of states, the quasiparticle spectral function, and the plasmon line shape. In spectroscopic experiments on real samples, additional phonon and disorder broadening as well as broadening due to extrinsic losses occur [28,29].

Also at nonzero wave vectors, the peak of $J_{\boldsymbol{k}}(\omega)$ is located at an energy ω_0 below the quasiparticle energy $E_{\boldsymbol{k}}$ (see Appendix). In other words: the satellite band is a rigidly shifted copy of the quasiparticle band. Surprisingly, this means that the *effective mass of the satellite is the same as the quasiparticle effective mass* irrespective of the plasmon effective mass. We confirm our conclusions by carrying out *GW*+C calculations of the 3DEG at $r_s = 4.0$ (corresponding to metallic sodium) using the frequency-dependent RPA dielectric function; see Fig. 1(b).

Generalizing our findings for the plasmon satellite properties of the 3DEG to real materials is straightforward. Figure 1(c) shows the spectral functions of crystalline silicon obtained from *ab initio GW*+C calculations [30]. Because of the parabolic dispersion of the valence quasiparticle bands near the band extrema and the parabolic dispersion of the plasmon, the plasmon satellite band structure appears as a rigidly shifted copy of the quasiparticle band structure, but significantly broadened.

Previous models of plasmon satellites in three-dimensional systems [6,31,32] assumed that plasmon dispersion is a minor effect and approximated the satellite simply as a shifted, broadened copy of the quasiparticle peak. Such approaches fail to describe the asymmetric line shape of the satellite and also cannot be applied straightforwardly to lower-dimensional systems, which we discuss below.

Plasmon satellites in two and one dimensions. In three-dimensional systems, the satellite feature is separated from the quasiparticle peak by the lowest plasmon frequency. In metallic *two-dimensional* systems, the plasmon energy is proportional to the square root of the plasmon wave vector, i.e., $\omega_{\boldsymbol{q}} = \beta\sqrt{q}$ [20], and it is not *a priori* clear where the satellite peak is located.

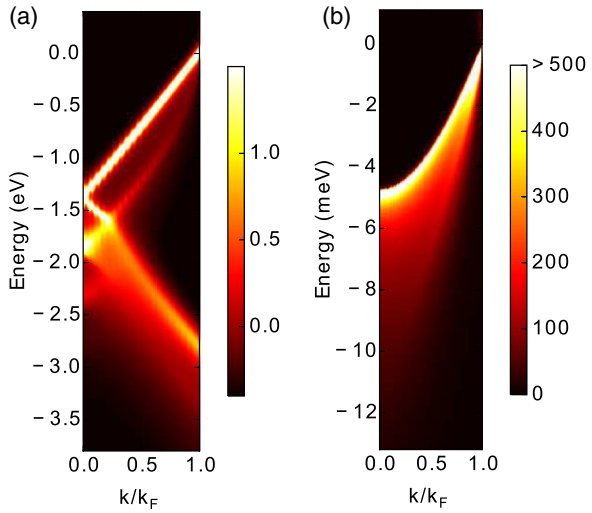

FIG. 2. (a) Spectral functions (in 1/eV) of doped graphene on a silicon carbide substrate from *GW* plus cumulant theory. (b) Spectral functions (in 1/eV) of a one-dimensional electron gas from *GW* plus cumulant theory.

We now apply our *GW*+C-based analysis of plasmon satellite properties to *two-dimensional systems* and choose electron-doped graphene as a test case. Within the Dirac model approach, the two bands in the vicinity of the Fermi energy are described by a linear dispersion relation, i.e., $E_{\boldsymbol{k}} = \pm v_F k$, with v_F denoting the graphene Fermi velocity. Here, $\boldsymbol{k}$ is measured from the K or K' points of the graphene Brillouin zone.

Taking into account that electrons in the upper Dirac band give the dominant contribution to the satellite spectral function at the Dirac point [33], we find that $J_{\boldsymbol{k}=0}(\omega) \propto \Theta(\omega + \tilde{\omega})/\sqrt{\omega + \tilde{\omega}}$, where $\tilde{\omega} = \beta^2/(4v_F)$ is the separation between the quasiparticle and satellite peaks. Again, the plasmon satellite line shape is highly asymmetric. The dependence of β on the charge density n, $\beta \propto \sqrt{n}$ [16], gives rise to small changes in the line shape as a function of the carrier density. Comparing the expression for $J_{\boldsymbol{k}=0}$ of doped graphene to the result for the 3DEG [see Eq. (10)], we observe that no drastic changes in the asymmetry of the line shape occur as function of the carrier density.

Figure 2(a) shows the spectral functions of doped graphene on a silicon carbide substrate from *GW*+C calculations [34]. We observe that the plasmon satellite band is not a shifted copy of the quasiparticle band, but that the two bands merge at the Fermi wave vector k_F.

Finally, we analyze the plasmon satellite properties in a *one-dimensional* metallic system, the 1DEG. In this system, the plasmon dispersion relation at long wavelengths is given by $\omega_{\boldsymbol{q}} = \beta q\sqrt{\ln(1/ql)}$ with l denoting a cutoff distance [35–37]. Assuming a parabolic quasiparticle dispersion, i.e., $E_{\boldsymbol{k}} = \alpha k^2$, we find again that the first plasmon satellite exhibits a highly asymmetric line shape. Figure 2(b) shows *GW*+C spectral functions for the 1DEG at $r_s = 1.4$ [38]. In contrast to graphene and the 3DEG, the plasmon satellite is relatively weak and appears as a shoulder-like feature near a strong quasiparticle band.

Summary. By connecting the *GW*+C Green's function approach to a wave-function-based perspective, we established the coupling-constant-weighted electron-plasmon joint density of states $J_{\boldsymbol{k}}(\omega)$ as a useful quantity for analyzing plasmon satellites in electron spectral functions. We evaluated $J_{\boldsymbol{k}}(\omega)$ for systems in one, two, and three dimensions and demonstrated how the properties of plasmon satellites are related to the properties of the underlying electrons and plasmons emphasizing the importance of plasmon dispersion. Our formalism for electron-plasmon interactions can be generalized straightforwardly to study the generation of hot electron-hole pairs in plasmonic devices for photovoltaics and photocatalysis in the future.

Acknowledgments. The authors would like to thank Prof. Feliciano Giustino for valuable discussions. J.L. acknowledges support from EPRSC under Grant No. EP/N005244/1 and also from the Thomas Young Centre under Grant No. TYC-101. Via J.L.'s membership in the UK's HEC Materials Chemistry Consortium, which is funded by EPSRC (EP/L000202), this work used the ARCHER UK National Supercomputing Service. S.G.L. acknowledges support by the SciDAC Program on Excited State Phenomena in Energy Materials funded by the U. S. Department of Energy (DOE), Office of Basic Energy Sciences and of Advanced Scientific Computing Research, under Contract No. DE-AC02-05CH11231 at Lawrence Berkeley National Laboratory (algorithm and code development) and by the National Science Foundation under Grant DMR15-1508412 (basic theory and formalism)

APPENDIX

Electron-plasmon joint density of states in three dimensions. We calculate the coupling-strength-weighted joint density of states $J_{\boldsymbol{k}}(\omega)$ comprising only plasmon-hole pairs with total momentum $\boldsymbol{k}$ for a three-dimensional homogeneous electron gas (3DEG). As shown in the main text, this quantity is closely related to the first satellite contribution to the electron spectral function. Specifically, $J_{\boldsymbol{k}}(\omega)$ is given by

$$J_{\boldsymbol{k}}(\omega) = \int \frac{d^3q}{(2\pi)^3} g_{\boldsymbol{q}}^2 \delta(\omega - E_{\boldsymbol{k}-\boldsymbol{q}} + \omega_{\boldsymbol{q}}), \tag{A1}$$

where $g_{\boldsymbol{q}}$ denotes the electron-plasmon coupling strength, $\omega_{\boldsymbol{q}} = \omega_0 + \beta q^2$ is the plasmon dispersion, and $E_{\boldsymbol{k}} = \alpha k^2$ is the quasiparticle dispersion.

Using a plasmon-pole model that conserves sum rules, we find $g_{\boldsymbol{q}}^2 = v_{\boldsymbol{q}}\omega_0^2/(2\omega_{\boldsymbol{q}}) \approx v_{\boldsymbol{q}}\omega_0/2$ with $v_{\boldsymbol{q}} = 4\pi/q^2$.

For the special case of $\boldsymbol{k} = 0$, we find

$$\begin{aligned} J_{\boldsymbol{k}=0}(\omega) &= \frac{\omega_0}{\pi}\int_0^\infty dq\,\delta(\omega + \omega_0 - [\alpha - \beta]q^2) \\ &= \frac{\omega_0}{2\pi}\frac{\Theta(\mathrm{sgn}(\alpha - \beta)(\omega + \omega_0))}{\sqrt{|(\alpha - \beta)(\omega + \omega_0)|}}, \end{aligned} \tag{A2}$$

which has a peak at $-\omega_0$.

In the general case of nonzero $\boldsymbol{k}$, we have to evaluate

$$\begin{aligned} J_{\boldsymbol{k}}(\omega) = \frac{\omega_0}{2\pi}\int_0^\infty dq \int_{-1}^1 du\,\delta(\omega + \omega_0 - \alpha k^2 \\ + 2\alpha k u + [\beta - \alpha]q^2). \end{aligned} \tag{A3}$$

Using that $\int_{-1}^{1} du\delta(A+Bu) = \Theta(|B|-|A|)/|B|$, we find that

$$J_{\boldsymbol{k}}(\omega) = \frac{\omega_0}{4\pi|\alpha|k}\int_0^\infty \frac{dq}{q}\Theta(2kq|\alpha| - |\omega + \omega_0 - \alpha k^2 + [\beta-\alpha]q^2|). \quad \text{(A4)}$$

We now assume that $\beta - \alpha > 0$ and distinguish the two cases: (i) $\omega_k^* \equiv \omega + \omega_0 - \alpha k^2 > 0$ and (ii) $\omega_k^* < 0$. To find the position of the peak of $J_{\boldsymbol{k}}(\omega)$, it is sufficient to consider case (i) and we find that

$$J_{\boldsymbol{k}}(\omega) = \frac{\omega_0}{4\pi|\alpha|k}\int_0^\infty \frac{dq}{q}\Theta(2kq|\alpha| - \omega_k^* - [\beta-\alpha]q^2) = \frac{\omega_0}{4\pi|\alpha|k}\Theta(1-f_k)\ln\left[\frac{1+\sqrt{1-f_k}}{1-\sqrt{1-f_k}}\right], \quad \text{(A5)}$$

with $f_k = [\beta-\alpha]\omega_k^*/(k|\alpha|)^2$. This function diverges as $\omega_k^* \to 0$ indicating that $J_{\boldsymbol{k}}(\omega)$ is peaked at $-[\omega_0 - \alpha k^2]$.

For case (ii), we have to evaluate

$$J_{\boldsymbol{k}}(\omega) = \frac{\omega_0}{4\pi|\alpha|k}\left[\int_0^{q^*}\frac{dq}{q}\Theta(2kq|\alpha| + \omega_k^* + [\beta-\alpha]q^2) + \int_{q^*}^\infty \frac{dq}{q}\Theta(2kq|\alpha| - \omega_k^* - [\beta-\alpha]q^2)\right] = \frac{\omega_0}{4\pi|\alpha|k}\ln\left[\frac{1+\sqrt{1-f_k}}{-1+\sqrt{1-f_k}}\right], \quad \text{(A6)}$$

with $q^* = \sqrt{|\omega_k^*|/[\beta-\alpha]}$.

Note that the solutions above also describe the case of $\beta - \alpha < 0$, but now Eq. (5) describes negative ω_k^* and Eq. (6) describes positive ω_k^*.

[1] S. Mukherjee, F. Libisch, N. Large, O. Neumann, L. V. Brown, J. Cheng, J. B. Lassiter, E. A. Carter, P. Nordlander, and N. J. Halas, Nano Lett. **13**, 240 (2012).
[2] C. Clavero, Nat. Photonics **8**, 95 (2014).
[3] M. Moskovits, Nat. Nanotechnol. **10**, 6 (2015).
[4] B. I. Lundqvist, Phys. Kondens. Mater. **9**, 236 (1969).
[5] J. Inglesfield, J. Phys. C **16**, 403 (1983).
[6] M. Guzzo, G. Lani, F. Sottile, P. Romaniello, M. Gatti, J. J. Kas, J. J. Rehr, M. G. Silly, F. Sirotti, and L. Reining, Phys. Rev. Lett. **107**, 166401 (2011).
[7] J. Lischner, G. K. Pálsson, D. Vigil-Fowler, S. Nemsak, J. Avila, M. C. Asensio, C. S. Fadley, and S. G. Louie, Phys. Rev. B **91**, 205113 (2015).
[8] M. Guzzo, J. J. Kas, L. Sponza, C. Giorgetti, F. Sottile, D. Pierucci, M. G. Silly, F. Sirotti, J. J. Rehr, and L. Reining, Phys. Rev. B **89**, 085425 (2014).
[9] L. Ley, S. Kowalczyk, R. Pollak, and D. Shirley, Phys. Rev. Lett. **29**, 1088 (1972).
[10] A. Bostwick, F. Speck, T. Seyller, K. Horn, M. Polini, R. Asgari, A. H. MacDonald, and E. Rotenberg, Science **328**, 999 (2010).
[11] O. E. Dial, R. C. Ashoori, L. N. Pfeiffer, and K. W. West, Phys. Rev. B **85**, 081306(R) (2012).
[12] A. L. Walter, A. Bostwick, K.-J. Jeon, F. Speck, M. Ostler, T. Seyller, L. Moreschini, Y. J. Chang, M. Polini, R. Asgari *et al.*, Phys. Rev. B **84**, 085410 (2011).
[13] D. C. Langreth, Phys. Rev. B **1**, 471 (1970).
[14] L. Hedin, Phys. Scr. **21**, 477 (1980).
[15] J. Lischner, D. Vigil-Fowler, and S. G. Louie, Phys. Rev. Lett. **110**, 146801 (2013).
[16] J. Lischner, D. Vigil-Fowler, and S. G. Louie, Phys. Rev. B **89**, 125430 (2014).
[17] F. Aryasetiawan, L. Hedin, and K. Karlsson, Phys. Rev. Lett. **77**, 2268 (1996).
[18] J. McClain, J. Lischner, T. Watson, D. A. Matthews, E. Ronca, S. G. Louie, T. C. Berkelbach, and G. K. Chan, arXiv:1512.04556 [Phys. Rev. B (to be published)].
[19] G. D. Mahan, *Many-Particle Physics* (Kluwer Academics/Plenum Publishers, New York, 2000).
[20] G. Giuliani and G. Vignale, *Quantum Theory of the Electron Liquid* (Cambridge University Press, New York, 2005).
[21] J. J. Kas, J. J. Rehr, and L. Reining, Phys. Rev. B **90**, 085112 (2014).
[22] L. Hedin, B. Lundqvist, and S. Lundqvist, Solid State Commun. **5**, 237 (1967).
[23] L. Hedin and S. Lundqvist, Solid State Phys. **23**, 1 (1969).
[24] B. I. Lundqvist, Phys. Kondens. Mater. **6**, 193 (1967).
[25] L. Hedin, J. Phys.: Condens. Matter **11**, R489 (1999).
[26] We neglect states with more than one plasmon excitation.
[27] K. Sturm, Adv. Phys. **31**, 1 (1982).
[28] C.-O. Almbladh and L. Hedin, in *Handbook of Synchroton Radiation*, Vol. 1 (North-Holland, Amsterdam, 1983), p. 686.
[29] L. Hedin, J. Michiels, and J. Inglesfield, Phys. Rev. B **58**, 15565 (1998).
[30] Our calculations employ a DFT-LDA mean-field starting point (obtained using the QUANTUM ESPRESSO program package [39]) and a full-frequency treatment of the dielectric matrix. Self-energy calculations were carried out using the Berkeley GW program package [40]. We employ a $8\times8\times8k$-point grid, a 5 Ry dielectric cutoff, and sampled frequencies up to 300 eV.
[31] F. Caruso and F. Giustino, Phys. Rev. B **92**, 045123 (2015).
[32] F. Caruso, H. Lambert, and F. Giustino, Phys. Rev. Lett. **114**, 146404 (2015).
[33] M. Polini, R. Asgari, G. Borghi, Y. Barlas, T. Pereg-Barnea, and A. H. MacDonald, Phys. Rev. B **77**, 081411 (2008).
[34] Our calculations employ a Dirac-model starting point and use the frequency-dependent RPA dielectric constant of doped graphene [41]. For the dielectric response of the silicon carbide substrate, we use the approach of Ref. [15]. The Fermi energy is $\epsilon_F = 1$ eV.
[35] A. Sommerfeld, Ann. Phys. **303**, 233 (1899).
[36] B. Y.-K. Hu and S. D. Sarma, Phys. Rev. B **48**, 5469 (1993).
[37] A. Chaplik and M. Krasheninnikov, Surf. Sci. **98**, 533 (1980).
[38] We employ a one-dimensional Coulomb interaction corresponding to a cylindrical system of radius 100 Å, an effective mass of $m^* = 0.067$ (in atomic units), and a background dielectric constant of 12.7 corresponding to a gallium arsenide quantum-wire structure [36] .
[39] P. Giannozzi *et al.*, J. Phys.: Condens. Matter **21**, 395502 (2009).
[40] J. Deslippe, G. Samsonidze, D. A. Strubbe, M. Jain, M. L. Cohen, and S. G. Louie, Comput. Phys. Commun. **183**, 1269 (2012).
[41] B. Wunsch, T. Stauber, F. Sols, and F. Guinea, New J. Phys. **8**, 318 (2006).